Thermodynamics of Several Lewis-Acid-Base Stabilized Transition Metal Alloys

JOHN K. GIBSON, LEO BREWER, and KARL A. GINGERICH

High-temperature (1425 to 2750 K) thermodynamic activities of one or both components of twenty-five binary alloys of a group IVB-VIB element (Ti, Zr, Hf, Nb, Ta, or W) with a platinum group element (Ru, Os, Ir, Pd, Pt, or Au) have been determined by equilibrating the alloy with the appropriate carbide and graphite, equilibrating with the nitride and nitrogen gas, or measuring the partial vapor pressure(s) thermogravimetrically or mass spectrometrically. The extraordinary stability of this class of transition metal alloy is attributed to a generalized Lewis-acid-base interaction involving valence *d* electrons, and the results of these investigations are interpreted within the context of this effect. Among the conclusions made are that a non-spherically-symmetrical crystal field significantly reduces the bonding effectiveness of certain valence *d* orbitals; the effect of the extent of delocalization of these orbitals is also considered.

I. INTRODUCTION

THE Engel correlation between crystal structures and electronic configurations[1] has been very successfully applied to the prediction of unary, binary, and higher order phase diagrams of the transition elements.[2] This theory recognizes the importance of valence *d* electron bonding, and extraordinary stability was anticipated in alloys which increase the net amount of such bonding relative to the pure constituent elements.[3] According to the Engel model, all of the transition elements to the right of group VIIB have more than five valence *d* electrons in their high-temperature solids and have one or more internally paired sets since only five valence *d* orbitals are available. Similarly, the transition elements to the left of group VIB all have high-temperature structures with less than five valence *d* electrons, and thus one or more of their corresponding orbitals are vacant. Since the internally paired valence electrons cannot participate in interatomic bonding in the pure element but could do so if an appropriate vacant valence orbital were available on a neighboring atom, it was predicted that donor-acceptor alloys between these two types of transition elements would be very stable.[3] Large negative free energies of formation have since been established for several such acid-base systems; $ZrPt_3$, for example, has a standard enthalpy of formation from the elements at 298 K of -128 kJ/g · atom[4] or $\Delta H°/R = -15.4$ kilokelvin.

Thermodynamic studies of several of these acid-base alloys have indicated extraordinary stability, but it is not entirely clear what factors are most important in determining the extent of this type of bonding. Large internal pressure and size differences will tend to destabilize intermetallic phases relative to the pure elements and reduce solubilities, but for the systems of interest here, these effects are expected to be small relative to the strong electronic effects involved. For reasons discussed below, the acid-base interaction is expected to be largest for the second and third transition series elements, and several of those from group IVB (Zr, Hf) through group IB (Ag, Au) as well as the first series element Ti were studied in the work reported here; for these elements, the internal pressures[2] (internal pressure = [energy of sublimation ÷ molar volume]) range from 416 (Pd) to 893 kilobar (Os), and their single bond metallic radii, given by Pauling,[5] range from 1.25 (Ru) to 1.45 Å (Zr).

Of the several parameters which may be expected to affect the magnitude of acid-base stabilization, one is certainly the degree of extension and bonding overlap of the valence *d* orbitals involved. Whereas *s*, *p* orbital bonding effectiveness generally decreases upon moving down a given group in the periodic table, the valence *d* orbitals become more delocalized relative to the closed electronic core and thus more strongly bonding.[6] Thus, the increase in internal pressure, for example down group VIB, is from 530 for Cr (3*d*) to 690 for Mo (4*d*) to 870 kilobar for W (5*d*).[2] Since it is *d* orbital bonding which stabilizes the alloys of interest here, it would be expected that third series (5*d*) alloys would be the most stable, second series (4*d*) alloys somewhat less so, and first series (3*d*) alloys even less strongly bonded. In accord with this, both galvanic cell[7] and calorimetry[4] measurements have shown increasing stability of APt_3 alloys when A is changed from Ti to Zr to Hf. Equilibrations of ZrC and graphite with binary Zr alloys of second and third series hyperelectronic transition elements (Re, Ru, Os, Rh, Ir, Pd, Pt, Ag, and Au)[8] established clear stability trends upon moving across each series of donor metals and generally gave greater stabilities for the 5*d* compared with the corresponding 4*d* alloy, but surprisingly suggested greater bonding of Ru (4*d*) than of Os (5*d*) with Zr. The investigations reported here have cleared up this apparent discrepancy and provide 3*d* *vs* 4*d* *vs* 5*d* acid-base effectiveness comparisons for additional systems.

Other possibly significant acid-base effectiveness parameters may be considered from the point of view of moving across a given transition series. Although standard electronegativity values, such as those given by Pauling,[5] are based upon metal-nonmetal compounds and are inapplicable to these alloys, some electronegativity effect will certainly be relevant. The nuclear charge outside of the

JOHN K. GIBSON, formerly Graduate Student Research Assistant, Materials and Molecular Research Division, Lawrence Berkeley Laboratory, and Department of Chemistry, University of California, Berkeley, is now with the Chemistry Division, Oak Ridge National Laboratory, Oak Ridge, TN 37830. LEO BREWER is Principal Investigator, Materials and Molecular Research Division, Lawrence Berkeley Laboratory, and Professor, Department of Chemistry, University of California, Berkeley, CA 94720. KARL A. GINGERICH is Professor, Department of Chemistry, Texas A and M University, College Station, TX 77843.

Manuscript submitted November 3, 1983.

closed electronic core (core includes all filled orbitals except the valence *s*, *p*, and *d*) may be considered as an approximate effective electronegativity which increases steadily across each series to the right so that, for example, the more electronegative Ta might be expected to be a stronger acid than neighboring Hf to its left. Conversely, the two vacant valence *d* orbitals available to body centered cubic (bcc) Hf would tend to make it a more effective acceptor of non-bonding electrons from a neighboring hyperelectronic element than bcc Ta with its single such vacant orbital. As a result of a non-spherically-symmetrical crystal field, the valence *d* orbitals will be of varying effectiveness in bonding with neighboring atoms and the least effective will remain unused and empty so that one of the two vacant Hf orbitals may be much more effective for bonding than the sole available orbital of Ta. This type of crystal field effect is clearly evident for the pure elements where the bonding enthalpy per bonding *d* electron reaches a distinct minimum when all five valence *d* orbitals are used in bonding.[6] The availability of two orbitals on Hf will clearly be most significant for especially electron-excess alloys where many non-bonding pairs are to be accommodated. Analogous considerations for donor metals predict a competition between decreasing nuclear charge/electronegativity to the left and a greater number of non-bonding valence electron pairs to the right. Several of the results reported here serve to establish the relative importance of these two effects and show clearly the effect of crystal field splitting on acid-base bonding.

The systems studied and the experimental methods used here were chosen to obtain thermodynamic information which may be interpreted in terms of the effects of the various factors discussed above on the degree of acid-base bonding in transition metal alloys. Results are presented for one or more binary alloys of each of the following combinations: Zr-Ru, Zr-Os, Hf-Os, Nb-Os, Ta-Os, W-Os, Ti-Ir, Zr-Ir, Hf-Ir, Ta-Ir, W-Ir, Zr-Pd, Hf-Pd, Nb-Pd, Ta-Pd, Ti-Pt, Zr-Pt, Hf-Pt, Nb-Pt, and Zr-Au.

II. EXPERIMENTAL

The thermodynamic activity of one of the components of each binary alloy studied was established by equilibrating the alloy with the appropriate carbide (MC) and graphite, by equilibrating with the nitride (MN) and nitrogen gas, or by measuring the partial vapor pressure of the component of interest above the alloy. In Table I are given the form and purity of each of the starting materials used. Alloys were prepared by arc-melting the rod, sheet, foil, or wire of the pure elements on a water-cooled copper hearth with a tungsten electrode, all under a titanium-gettered argon atmosphere. Each alloy button was flipped and remelted several times to ensure homogeneity, and a net weight was obtained before and after melting to ensure that no significant loss had occurred due to vaporization. All experimental temperature measurements were with 653 nm optical pyrometers which had been calibrated against the 1968 International Practical Temperature Scale.

A. *Carbide Equilibration*

This approach is essentially identical to that used previously by Brewer and Wengert.[8] The object of these experiments was to establish the three-phase equilibrium between some acid-base alloy M_xPl_{1-x} (M = Ti, Zr, Hf, V, Nb, Ta, or W; Pl = Ru, Os, Rh, Ir, Pd, Pt, Ag, or Au), the corresponding carbide MC, and graphite. An incomplete 1800 °C section of the typical Ta-Ir-C phase diagram is given in Figure 1; only the three phase field of immediate interest is shown, although all binary phases are indicated along the edges.[9] At equilibrium, the thermodynamic activity, a_i, of all components must be identical in each phase and that of the acid metal component, here Ta, is related to the standard free energy of formation of its carbide through:

$$\Delta G_f^\circ \text{ (TaC)} = RT \ln[a_{Ta} \cdot a_C \cdot a_{TaC}^{-1}].$$

If the net composition is chosen such that graphite and the near-stoichiometric carbide are present after equilibration with the acid-base alloy, then their activities are each essentially unity using the pure solvent standard state (as will be done throughout this paper), and the activity of the acid metal in the alloy is obtained from the above relation. In Table II are given the partial molar free energies of the acid metal in its carbide in equilibrium with graphite at a typical equilibration temperature of 2200 K; values at other temperatures were obtained from the indicated references and have the same uncertainties as given.

Powders of the carbide (MC), pure platinum group metal (Pl), or brittle alloy (M_xPl_{1-x}) which had been pulverized in

Table I. Starting Materials

Carbide Equilibration	Nitride Equilibration	Vapor Pressure
ZrC, −325 mesh powder, 99 pct	TiN, −325 mesh powder, 99.5 pct	Ti, rod, 99.97 pct
HfC, −325 mesh powder, 99 pct	ZrN, −325 mesh powder, 99 pct	Zr, rod, 99.94 pct
NbC, −325 mesh powder, 99.8 pct	HfN, −200 mesh powder, 99.8 pct	Hf, rod, 99.97 pct
TaC, powder, 99.95 pct	NbN, −325 mesh powder, 99.5 pct	Nb, rod, 99.97 pct
WC, −325 mesh powder, 99 pct	nitrogen, gas, 99.996 pct	Ta, foil, 99.9 pct
graphite, −200 mesh powder, 99.999 pct	Pd, sheet, 99.95 pct	Ir, wire, 99.9 pct
Ru, −60 mesh sponge, 99.8 pct	Pt, sheet, 99.95 pct	Pd, rod, 99.99 pct
Os, −60 mesh powder, 99.9 pct	Zr, rod, 99.94 pct	Au, wire, 99.99 pct
Ir, powder, 99.7 pct	Nb, rod, 99.97 pct	
Pd, −325 mesh powder, 99.8 pct		
Pt, +100 mesh powder, 99.9 pct		
Pd, sheet, 99.95 pct		
Pt, sheet, 99.95 pct		
Zr, rod, 99.94 pct		
Nb, rod, 99.97 pct		

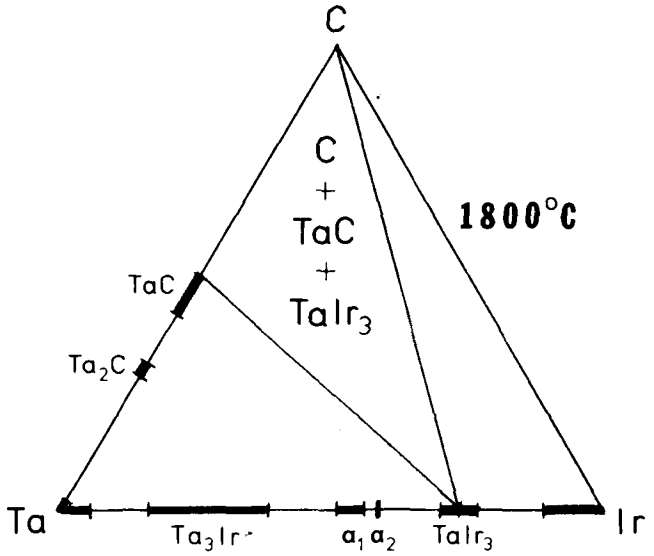

Fig. 1—Ta-Ir-C 1800 °C isothermal section showing relevant three-phase region for carbide equilibrations.

Table II. Carbide Thermodynamics

Carbide	$\Delta\bar{G}_M/R$ (MC + graphite), 2200 K Kilokelvin	Reference
WC	− 7.5 ±2	10
NbC	−16.6 ±1.5	11
TaC	−17.0 ±1.5	12
ZrC	−21.6 ±1.5	13
HfC	−25.6 ±1.5	14,15

a hard steel mortar and pestle, and in some cases graphite (C), were weighed out to provide a net composition in the MC-C-M_xPl_{1-x} three-phase region, and thoroughly mixed in glass jars. Approximately 3 gm of the mixture was then transferred to a 3.81 cm o.d., 1.27 cm i.d., 3.81 cm tall die of 99.5 pct ATJ-grade graphite and placed into a uniaxial hot-press with a tungsten resistance heating element and tantalum heat shielding. In a vacuum chamber maintained at 10^{-7} atm* or less, all solid-state equilibrations were carried out under 480 atm uniaxial pressure to ensure good contact between the reactant powders, while the few runs which involved liquid alloys were carried out with no applied pressure. Temperature measurements were made by sighting through a shutter-protected quartz window onto the top of the die; window attenuation corrections of up to +20° (at 2200 °C) and emissivity corrections by the method of Battuelo and Ricolfi[19] using an emissivity of rough graphite of 0.79[20] of up to +48° were applied to all measured temperatures. Due to these corrections and the distance of the sample from the surface whose temperature was measured, a net temperature uncertainty of up to ±100° is assigned. This large value is acceptable in view of the relative temperature insensitivity of these equilibria as certain of the results will illustrate.

*Throughout this paper, 1 atm = 1.013×10^5 pascal.

At the conclusion of the 1 to 5 hour equilibration period the power to the heating elements was abruptly terminated and rapid cooling ensued, typically from 1900 °C to 1500 °C within 30 seconds, and to 1000 °C within 150 seconds, so that re-equilibration during cooling of the solids should have been negligible. In Figure 2 is shown an optical micrograph of an equilibrated WC-C-Os(W) pellet which has been polished on SiC paper followed by 1 μ alumina-water paste on a felt polishing wheel.

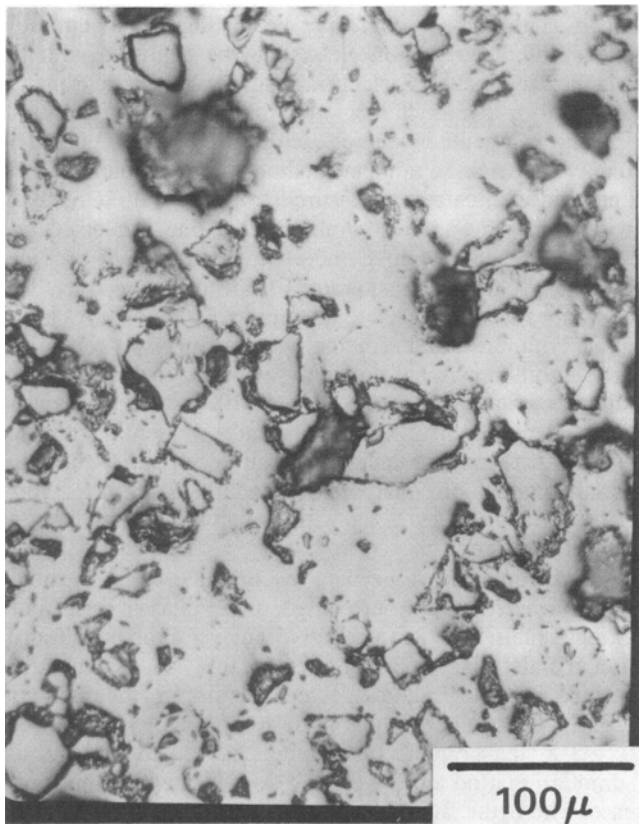

Fig. 2—Optical micrograph of WC-C-Os (W) three-phase system after high-temperature equilibration.

Analyses: An X-ray diffractometer using Fe K_α or Cu K_α radiation was used to obtain X-ray diffraction (XRD) patterns[32] for each of the polished pellet surfaces, all of which had essentially the same appearance as the WC-C-Os(W) system shown in Figure 2. The diffraction patterns confirmed the existence of graphite[21] and the appropriate binary carbide[22-25] and indicated that the third phase was either an intermetallic of stoichiometry MPl_3 or a terminal solid solution of the carbide (acid) metal in the platinum group metal. In accord with the low affinity of the platinum group metals for carbon and the known phase relations in the Ti-Ru-C and Ti-Pt-C systems[26] which are expected to behave similarly to those studied here, no ternary carbides were ever detected by XRD. The compositionally narrow intermetallics identified by their diffraction patterns were $HfIr_3$,[27] $ZrIr_3$,[28] $TaPd_3$,[29] $ZrPt_3$,[30] $ZrPd_3$,[27] and $TaIr_3$.[27]

All other alloys were solid solutions and were analyzed by electron probe microanalysis (EPMA) using an eight channel A.R.L. instrument which is interfaced with a microcomputer and uses the MAGIC IV program[31] to correct raw X-ray emission counts for absorption and fluorescence excitation of each line and average atomic number effects on electron energy loss and backscattering.[33] A LiF, ADP, or TAP crystal monochrometer was tuned to the L_α (K_α for Ti;

the α_1 and α_2 lines could not be distinguished) emission energy of the transition element to be analyzed with the channel and a 20 kV electron beam of a few microns diameter focused onto the region of the sample to be analyzed. Background count levels for each element were obtained by the average atomic number method whereby counts for the analyzed elements are measured from several elements of widely varying atomic number and a linear interpolation to the average atomic number of the unknown provides the background to be subtracted from the raw counts. Uncertainties were assigned to the reported compositions based upon both the scatter in the several analyses performed on each unknown and the analyses of arc-melted alloys of known composition using the same 100 pct standards used for the unknowns. Although dilute elemental analyses (<3 at. pct) may be uncertain by up to 50 pct of the measured composition, analyses of standard alloys in the composition range 25 to 75 at. pct were always accurate to ±2 to 3 at. pct.

EPMA analysis of a typical equilibrated pellet as shown in Figure 2 revealed the requisite three phases: small pure graphite particles (*i.e.*, negative analyses for both transition metals), larger bright alloy grains, and surrounding carbide matrix (*i.e.*, negative analysis for the platinum group metal). That no platinum group metal was ever detected in the graphite or carbide phases supports the assumption that no ternary phases were formed. In the single case where the acid metal concentration was below the EPMA detection limit (Zr-Os), an upper limit was estimated using a statistical treatment of background and standard X-ray count levels.[34]

B. *Nitride Equilibration*

In Figure 3 is shown the relevant three phase field on the Gibbs triangle for the typical example of the ZrN-Pt(Zr)-N_2 equilibrium at 2200 °C. Again, the thermodynamic activities are identical in each phase in equilibrium, and here the acid metal activity is related to the nitride free energy of formation through:

$$\Delta G_f^\circ(\mathrm{ZrN}) = RT \ln [a_{\mathrm{Zr}} \cdot P_{\mathrm{N_2}}^{1/2} \cdot a_{\mathrm{ZrN}}^{-1}].$$

Since the pure nitride is present at close to unit activity, the zirconium activity may be expressed in terms of $\Delta G_f^\circ(\mathrm{ZrN})$ and $P_{\mathrm{N_2}}^{1/2}$; by varying the nitrogen pressure, a_{Zr} may be controlled and a range of Zr-Pt alloy compositions should be accessible. In practice, the square root dependence and limited pressure range available for equilibrations severely limit the composition range which may be investigated for these very stable systems. These equilibrations were carried out above the alloy liquidus temperature so that the 1900 °C Zr-Pt binary section is shown in the figure to illustrate the behavior upon cooling the fully miscible liquid alloy to a two-phase solid. That the nitride had taken up a negligible amount of the platinum group metal was always verified by EPMA, and that the platinum group metal should have largely excluded nitrogen from the liquid alloy is suggested by the fact that no nitrides of these elements are known to exist. Rhenium is expected to have a greater affinity for nitrogen than the Pt and Pd used here, but the addition of 20 at. pct Re to Nb increases the activity coefficient of nitrogen at 2500 K by a factor of 6.3 relative to pure Nb.[35]

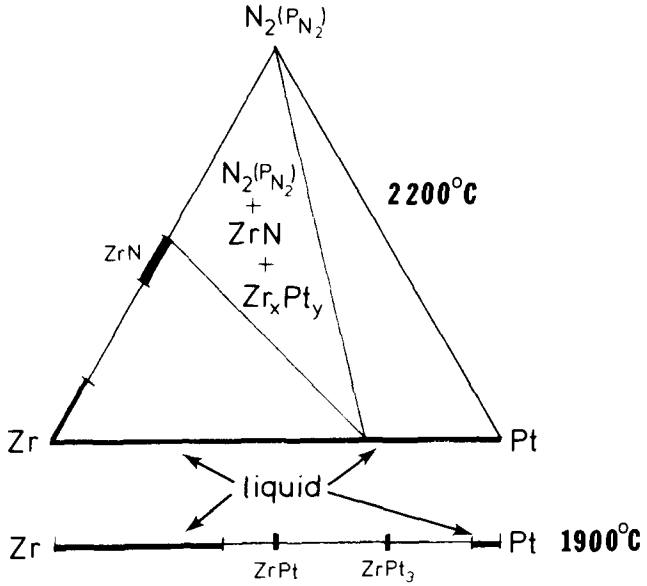

Fig. 3—Zr-Pt-N_2 2200 °C isothermal section showing relevant three-phase region for nitride equilibrations; binary 1900 °C Zr-Pt section.

Under a nitrogen atmosphere, TiN, ZrN, HfN, and NbN were each equilibrated with Pt, and NbN was also equilibrated with Pd. The thermodynamic quantities for the near-stoichiometric nitrides were obtained from the references indicated in Table III. As is readily apparent from the thermodynamic quantities shown there, the very large negative heats of formation of the nitrides are largely offset by the negative entropies involved in their formation; this effect is particularly pronounced at the high temperatures used for these equilibrations. The relative insensitivity of the equilibria to $P_{\mathrm{N_2}}$ variations of up to two orders of magnitude suggests that nitride stoichiometry was not a significant factor within the resolution of these experiments. A 0.2 to 0.6 mm thick disc of either the pure platinum group metal or an alloy of it with the nitride metal was cold-pressed into the center of a few grams of the nitride powder at 6800 atm in an 11 mm inside diameter hard steel die. The 2 wt pct naphthalene which was used as a binder was vaporized at 180 °C in a vacuum oven after grinding off any surface impurities with SiC paper. Equilibrations were carried out in a graphite tube resistance furnace[36] with the nitride pellet resting on a 99.95 pct tungsten foil liner inside of the tube; only minor surface adhesion to the tungsten occurred at even the highest temperatures used, and no contamination of the bulk nitride or alloy was ever detected by EPMA.

Temperature measurements were by sighting onto the pellet surface through quartz windows in each end of the furnace. Window attenuation corrections of up to +25° at

Table III. Nitride Thermodynamics

Nitride	$(\Delta H^\circ_f/R)_{298}$ Kilokelvin for 1 Mole MN	$\Delta\bar{G}_M/R$ (MN, 1 atm N_2) Kilokelvin at 2400 K	Ref.
NbN	−28.1 ±0.2	− 5.5 ±2	10, 16
TiN	−40.7 ±0.5	−14.2 ±2	17
ZrN	−44.3 ±0.4	−17.1 ±1	18
HfN	−45.0 ±0.4	−20.2 ±2.5	14, 15

2500 °C and emissivity corrections[19,20] of up to +77° (for TiN at 2370 °C) were applied to all temperature readings. Simultaneous measurement of the temperature on opposite sides of a pellet often suggested temperature gradients of up to 100° across 10 mm, so that an average temperature was used and an uncertainty of up to ±100° is considered typical. This large uncertainty is again acceptable in view of the invariance of the equilibrium alloy composition within the accuracy of these experiments over a range of several hundred degrees. The low nitrogen pressures (0.1 to 1.1 atm) were measured to ±0.004 atm with a mercury manometer corrected to the density at 0 °C while the high nitrogen pressures (10 to 12 atm) were measured to ±0.03 atm with a Bourdon-type mechanical gauge.

At the end of the 2 to 10 hour equilibration period the power to the furnace was shut off and a typical sample cooling rate was from 2000 °C to 1400 °C within 30 seconds and to below 1000 °C within 150 seconds. After the pellet was cut in half, the exposed surface was polished on SiC paper, followed by 1 μ alumina-water paste on a felt polishing wheel. In Figure 4 is shown a typical optical micrograph of such a pellet surface—small bright alloy grains (here Zr-Pt) surrounded by the dark nitride matrix (here ZrN). The pure metal or alloy had always melted and crept into and wetted the nitride particles. Since the quenched liquid alloys generally resulted in two-phase solids (see Figure 3), X-ray diffraction could not provide quantitatively accurate analyses, and all alloy compositions were obtained by EPMA, as described above. The slightly larger uncertainties assigned to these analyses are due primarily to interference from nitride inclusions in the relatively small alloy grains.

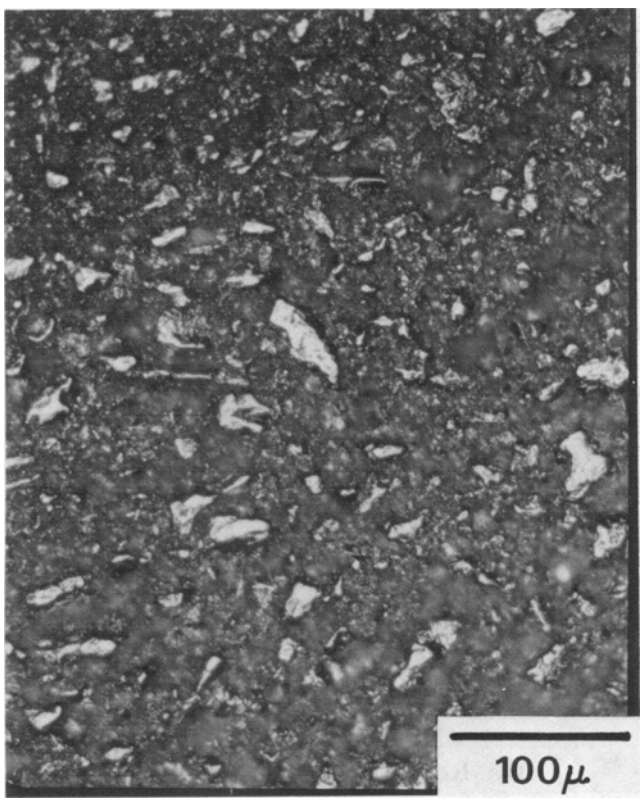

Fig. 4—Optical micrograph of ZrN-Pt(Zr) two-phase system after equilibration at high temperature under nitrogen.

C. *Thermogravimetric Vapor Pressure*

The total weight loss from a Knudsen cell containing a binary alloy of Pd, Au, or Ti with an element whose volatility is at least four orders of magnitude lower, up to 2100 K (Zr, Hf, Nb, or Ta with Pd; Zr with Au; Ir with Ti),[37] is related to the vapor pressure of the volatile component over the acid-base alloy. Given that the low-pressure/high-temperature conditions of these experiments should result in near-ideal gas behavior, the thermodynamic activity of component i, a_i, is related to the pressure, P_i, relative to the pure solvent state pressure, P_i°, by:[38]

$$a_i = P_i/P_i^\circ .$$

Several pieces (1 to 3 gm) of the pulverized alloy rich in the volatile component were placed into a graphite Knudsen cell of purity 99.7 pct or 99.99 pct as indicated with the results. The 0.95 to 1.27 cm o.d., 0.8 to 2.0 gm cells had orifices of diameter 0.23 to 0.29 cm, all measured to ±0.005 cm, and orifice edges generally on the order of 10 pct and always less than 20 pct of the diameter, so that a unit Clausing factor[39] was assumed. The Ti_3Ir alloy was run in a 99.5 pct ThO_2 crucible for which no lid was available, so that its inside diameter was used as the "orifice diameter." Certain samples were run simultaneously in a graphite holder into which two or more Knudsen cells may be placed adjacent to one another. After weighing to ±0.1 mg, the cell(s) were placed into a furnace with a tungsten resistance heating element and tantalum heat shields. The alloy-containing cell was maintained at the weight loss temperature for 1 to 22 hours with the furnace chamber pressure maintained at 10^{-7} atm or less. Temperatures were obtained by sighting into the Knudsen cell through a quartz shutter-protected window in the furnace wall; the cell interior was taken to be close to a blackbody, so that only window attenuation corrections of up to +15° were applied to the temperature readings. This correction, the pyrometer accuracy reported by the manufacturer, and the possibility of vertical and/or horizontal gradients within a cell, result in a net temperature uncertainty assignment of up to ±30°; relative temperatures for two or more alloys run simultaneously are taken to be accurate to at least ±20°. For pure Pd at 1800 K,[37] an uncertainty of ±30° implied a pressure uncertainty of ±1.5× (*i.e.*, a range of $P/1.5$ up to $1.5P$), while an uncertainty of ±20° would imply an uncertainty in the pressure of ±1.3×.

The cool cell(s) were reweighed and 1 mg was subtracted from the measured loss(es) to obtain the loss(es) from the alloy(s), since runs with blank (*i.e.*, empty) cells resulted in weight losses of 0.5 to 2.0 mg; and a net uncertainty of ±1 mg is assigned to the reported losses. Alloy vapor pressures were always below 2×10^{-4} atm, so that effusion should have been by molecular flow.[40] Further assuming that the vaporization coefficients from the alloys are close to unity,[41] that the non-volatile component makes a negligible contribution to the total weight loss rate (dw/dt), and that the Clausing factor is unity, then the pressure of the volatile component (P_M) is given by the molecular effusion formula of Knudsen:[42]

$$dw/dt_{(gm/sec)} = 44.32 \cdot P_{M(atm)} \cdot A_{(cm^2)} \cdot [M_{M(gm/mol)} \div T_K]^{1/2}$$

where A is the area of the cell orifice and M_M is the molecular weight of the effusate. Attempts were made to obtain an

internal calibration by running a pure Pd-containing cell adjacent to alloy cells. Vapor pressures obtained for solid Pd run in graphite, and for liquid Pd run in alumina, were in reasonable agreement with the literature values,[37] but liquid Pd vaporized from graphite cells repeatedly gave very low apparent pressures. Liquid Pd dissolves appreciable amounts of carbon,[43] and the low vaporization coefficient effect may have been related to reprecipitation of dissolved carbon as graphitic sheets on the liquid surface; all of the alloys studied included a carbide-forming element, and this behavior is not anticipated there. In lieu of an internal calibration, the standard state vapor pressures for pure Pd, Au, and Ti were obtained from Hultgren, *et al.*,[37] and are taken to be accurate to at least ±30 pct.

Due to vaporization of the volatile component, each experiment was on an alloy of some composition range as indicated with the results as an average composition with an associated uncertainty range of from ±0.1 to ±19 at. pct. These assigned compositions do not consider the effect of carbide formation, which could be at least partially counteracting for the Pd and Au alloys in graphite cells (especially for liquid alloys). A distinct carbide layer between the alloy and cell wall was indicated by EPMA after a liquid Nb-Pd alloy had been run in graphite. Creeping of the liquid alloy up the cell wall and even out through the orifice was frequently a problem, and only results from runs where this effect was minimal are reported. Reasonable agreement between solid and liquid runs for Nb-Pd and Zr-Au alloys established that surface depletion of the volatile component from the solid was not a significant problem; EPMA compositional profiles of post-run solid alloys did not detect any depletion to the few micron resolution of the microprobe.

D. *Mass Spectrometric Vapor Pressure*

The vapor pressure of Pd over three Nb-Pd alloys was determined by high-temperature mass spectrometry. Both the general experimental method and the particular design and operation of the Nuclide 12-90HT mass spectrometer used have been described previously by Gingerich.[44,45] To obtain the partial pressure of a species over the alloy, the effusate from a Knudsen cell was partially ionized by an electron beam, and the ion current of the singly ionized species of interest, I_M^+, was measured with an ion detector/electron multiplier. Then the pressure is given by:

$$P_M = k_M \cdot I_M^+ \cdot T$$

where k_M is a calibration constant which depends upon the geometry of the Knudsen cell, alignment of the cell with the ion source, and the absolute instrument sensitivity. Calibration constants were obtained at the start of each run by vaporizing approximately 10 mg of Ag wire and monitoring I_{Ag}^+ and $I_{Ag_2}^+$ at several temperatures in the range of 1050 to 1400 K. Insertion of I_{Ag}^+, T, and the known Ag vapor pressure,[37] P_{Ag}°, into the above expression yields k_{Ag}, while the Ag/Ag_2 data may be used to obtain a calibration constant through consideration of the equilibrium constant relating P_{Ag} and P_{Ag_2} to one another.[44] Using the dissociation energy and free energy functions for Ag_2 given by Hilpert and Gingerich[46] and the free energy functions for Ag from Hultgren, *et al.*,[37], the latter method usually gave values for k_{Ag} within 40 to 50 pct of those provided by the generally more reliable vapor pressure method. The k_{Ag} used were chosen with an emphasis on the P_{Ag}° data and are considered reliable to about ±1.5×. From k_{Ag} the calibration constant for another species, M, was obtained from

$$k_M = k_{Ag} \cdot [\sigma_{Ag}/\sigma_M] \cdot [\gamma_{Ag}/\gamma_M] \cdot [E_{Ag}/E_M] \cdot [n_{Ag}/n_M]$$

where the ionization cross-sections (σ_i) were taken from Mann,[47] the multiplier gains (γ_i) were measured, the relative ionization efficiencies (E_i) were found to be close to unity for all species monitored at the ionizing energy of 20 eV, and the isotopic abundances (n_i) are accurately known.

Graphite Knudsen cells of at least 99.7 pct purity were used for the 18 and 50 at. pct Nb-Pd alloys while a 99.8 pct NbC cell was used for the 80 at. pct Nb-Pd system, in anticipation of a relatively high Nb activity. The cells had 0.102 cm (18 at. pct Nb-Pd) or 0.254 cm diameter orifices with the larger ones used to increase sensitivity to the refractory Nb alloy component. Several pieces of the alloy amounting to 300 to 500 mg were loaded into the cell, and it was placed into a Ta casing and into the furnace. Heating was by an inductively wound, thoriated tungsten resistance element surrounded by tungsten and tantalum heat shields. Temperature measurements were by sighting into a blackbody hole in the bottom of the tantalum case and applying a window/prism attenuation correction. Earlier trial runs with this sample configuration[45] had shown the temperature gradients along the cell to be less than 10° up to 2350 K. A net temperature uncertainty of ±20° is considered reasonable up to 2300 K, and the activities reported are taken to be accurate to within a factor of two.

Differential pumping provided vacuums of $\sim 10^{-9}$ atm in the Knudsen cell region, $\sim 10^{-10}$ atm in the ion source region, and $\sim 10^{-11}$ atm in the ion analyzer region throughout each run. The ion accelerating voltage was held constant at 3 kV, and currents of ions of various mass/charge values were monitored by varying the magnetic field. Electron multiplier gains were obtained at relatively high ion currents by simultaneously monitoring the outputs from a 50 pct transmission grid and the 20-stage Cu-Be dynode multiplier. Currents were allowed to stabilize to a constant level after each temperature increase or decrease; the melting point of the 82 at. pct Pd-Nb alloy was established by small halts in the I_{Pd}^+ *vs* time (temperature) curves upon heating and cooling. Continuity of the vapor pressure through the liquidus indicates that surface depletion of Pd from the solid was not a problem. EMPA analyses of the post-run alloys alongside unused starting alloy indicated severe net Pd depletion for the 20 at. pct Pd-Nb to <1 at. pct Pd—this effect was clearly evident from the pressure data, and the low temperature results are emphasized below. While the 50 at. pct Pd-Nb system showed only minor depletion (a few at. pct), the 82 at. pct Pd-Nb alloy also showed a significantly lower post-run Pd concentration, but this effect is considered to be due to prolonged operation at elevated temperature after taking the data reported here. Pressures for the refractory Nb component were obtained only above 2100 K on the rapidly Pd-depleting "20 at. pct Pd-Nb" alloy.

III. RESULTS AND DISCUSSION

The Carbide Equilibration, Nitride Equilibration, and Thermogravimetric Vapor Pressure results are given in

Tables IV, V, and VI, respectively, and the Mass Spectrometric Vapor Pressure results are presented graphically as an Arrhenius plot in Figure 5. For the carbide and nitride experiments, the reactants and equilibration parameters (temperature, time, and P_{N_2} for the nitride runs) are given followed by the equilibrium alloy composition as determined by XRD (for the MPl_3 intermetallics) or by EPMA. The partial molal free energy of the carbide or nitride metal in the alloy ($\Delta\bar{G}_M = RT \ln a_M$) and the corresponding partial molal excess free energy ($\Delta\bar{G}_M^{xs} = \Delta\bar{G}_M + T\Delta\bar{S}_M^{id} = RT \ln a_M - RT \ln X_M = RT \ln \gamma_M$) are given with appropriate uncertainties. Since the excess quantity does not include the ideal configurational entropy stabilization term, it provides the best measure of the bonding effects of interest. For the thermogravimetric experiments, the alloy with composition range established by depletion of the volatile component, the cell material, the temperature, mass loss (corrected for blank losses; 1 mg subtracted from actual losses except for run V17 with ThO_2), and the pressure calculated using the Knudsen effusion equation are all given. Also shown are the activities calculated using the $P°$ for Pd, Au, and Ti from Hultgren, *et al.*,[37] and the partial

Table IV. Carbide Equilibrium Results

Reactant Mixture	T (K)	Equilib. Time (H)	Equilib. Alloy with MC + Graph.	$\Delta\bar{G}_M/R$ Kilokelvin	$\Delta\bar{G}_M^{xs}/R$ Kilokelvin
C1. 3.0 Ir + 1.0 HfC	2133	1	$HfIr_3$ (no HfC)	$<-26.0 \pm 1.5$	$<-23.0 \pm 2.0$
C2. 2.0 Pt + 1.0 ZrC	1905	3	$ZrPt_3$	-23.1 ± 1.5	-20.5 ± 2.0
C3. 1.9 Ir + 1.0 ZrC	1915	3	$ZrIr_3$	-23.0 ± 1.5	-20.3 ± 2.0
C4. 2.0 Pt + 1.0 ZrC	1926	3	$ZrPt_3$	-23.0 ± 1.5	-20.3 ± 2.0
C5. from run #3*	2321	2	$ZrIr_3$	-21.0 ± 1.5	-17.8 ± 2.0
C6. from run #4*	2300	2	$ZrPt_3$	-21.2 ± 1.5	-18.0 ± 2.0
C7. 2.0 Ir + 1.0 TaC	2154	3	$TaIr_3$	-17.1 ± 1.5	-14.1 ± 2.0
C8. 2.0 Pd + 1.0 TaC	1786	4.5	$TaPd_3$	-17.1 ± 1.5	-14.6 ± 2.0
C9. 1.0 ZrPt + 2.7 C	2061	4	$ZrPt_3$	-22.3 ± 1.5	-19.4 ± 2.0
C10. 1.0 $ZrPt_{.8}$ ($ZrPt + Zr_5Pt_3$) + 3.1 C	2019	3	$ZrPt_3$	-22.5 ± 1.5	-19.7 ± 2.0
C11. 1.9 Os + 1.0 TaC	2170	4	1.0 ±0.4 at. pct Ta-Os	-17.1 ± 1.5	-7.1 ± 2.5
C12. 1.7 Ir + 1.0 WC + ? C	2237	4	9.5 ±2 at. pct W-Ir	-7.9 ± 2.0	-2.7 ± 2.5
C13. 2.3 Os + 1.0 ZrC + ? C	2216	4	<0.1 ±0.05 at. pct Zr-Os	-21.5 ± 1.5	$> 6.2 \pm 3.0$
C14. 2.0 Os + 1.0 HfC + ? C	2211	4	0.3 ±0.2 at. pct Hf-Os	-25.6 ± 1.5	-12.8 ± 4.0
C15. 2.0 Os + 1.0 NbC + ? C	2196	4	0.8 ±0.3 at. pct Nb-Os	-16.6 ± 1.5	-6.0 ± 2.5
C16. 2.0 Os + 1.0 WC + ? C	2216	4	0.4 ±0.2 at. pct W-Os	-7.8 ± 2.0	4.4 ± 4.0
C17. 1.9 Ru + 1.0 ZrC + 1.0 C	2061	2	0.1 ±0.05 at. pct Zr-Ru	-22.3 ± 1.5	-8.0 ± 3.0
C18. 2.0 Pd + 1.0 NbC + 0.6 C*	2321	1.5	15 ±2 at. pct Nb-Pd	-16.5 ± 1.5	-12.2 ± 2.0
C19. 4.0 NbPd + 1.1 NbC + 0.6 C*	2268	2	15 ±2 at. pct Nb-Pd	-16.5 ± 1.5	-12.2 ± 2.0
C20. 2.0 Pd + 1.0 NbC + 0.6 C*	2331	2	16 ±2 at. pct Nb-Pd	-16.5 ± 1.5	-12.2 ± 2.0

*No applied uniaxial pressure

Table V. Nitride Equilibrium Results

Reactants	P_{N_2} (atm)	T(K)	Equilib. Time (H)	Equilib. Alloy	$\Delta\bar{G}_M/R$ Kilokelvin	$\Delta\bar{G}_M^{xs}/R$ Kilokelvin
N1. Pt + NbN	0.99	2594	2	50 ±4 at. pct Nb-Pt	-4.3 ± 2.0	-2.5 ± 2.0
N2. Pt + ZrN	1.11	2392	4	28 ±3 at. pct Zr-Pt	-17.3 ± 1.0	-14.3 ± 1.0
N3. Pt + ZrN	0.98	2371	8	27 ±3 at. pct Zr-Pt	-17.4 ± 1.0	-14.3 ± 1.0
N4. Zr_3Pt_2 + ZrN	0.96	2314	8	17 ±3 at. pct Zr-Pt	-18.0 ± 1.0	-15.0 ± 1.0
N5. Pt + ZrN	11.2	2350	8	29 ±3 at. pct Zr-Pt	-20.6 ± 1.0	-17.7 ± 1.0
N6. Pt + ZrN	11.2	2536	4	28 ±3 at. pct Zr-Pt	-18.5 ± 1.0	-15.3 ± 1.0
N7. Pt + ZrN	1.00	2159	8	30 ±3 at. pct Zr-Pt	-20.0 ± 1.0	-17.4 ± 1.0
N8. Pt + ZrN	0.114	2361	8	28 ±3 at. pct Zr-Pt	-15.0 ± 1.0	-12.0 ± 1.0
N9. Pt + TiN	1.00	2440	8	28 ±3 at. pct Ti-Pt	-13.8 ± 2.0	-10.7 ± 2.0
N10. Pt + TiN	11.1	2414	9.5	29 ±3 at. pct Ti-Pt	-17.0 ± 2.0	-14.0 ± 2.0
N11. Pt + TiN	0.157	2461	8	32 ±3 at. pct Ti-Pt	-11.3 ± 2.0	-8.5 ± 2.0
N12. Pt + TiN	11.0	2683	6.5	31 ±3 at. pct Ti-Pt	-14.4 ± 2.0	-11.3 ± 2.0
N13. Pt + TiN	1.00	2720	6	30 ±3 at. pct Ti-Pt	-10.8 ± 2.0	-7.5 ± 2.0
N14. Pt + HfN	11.1	2432	9.5	25 ±4 at. pct Hf-Pt	-22.9 ± 2.5	-19.5 ± 3.0
N15. Pt + HfN	0.99	2427	8	24 ±4 at. pct Hf-Pt	-20.0 ± 2.3	-16.5 ± 3.0
N16. Pt + HfN	11.1	2783	4	33 ±4 at. pct Hf-Pt	-19.5 ± 2.5	-16.4 ± 3.0
N17. Pt + HfN	0.99	2756	4	26 ±3 at. pct Hf-Pt	-16.4 ± 2.5	-12.6 ± 3.0
N18. NbPd + NbN	0.98	2406	4	34 ±3 at. pct Nb-Pd	-5.4 ± 2.0	-2.8 ± 2.5
N19. Pd + NbN	0.99	2406	4	34 ±3 at. pct Nb-Pd	-5.4 ± 2.0	-2.8 ± 2.5
N20. NbPd + NbN	10.8	2422	4	27 ±3 at. pct Nb-Pd	-8.2 ± 2.0	-5.0 ± 2.5

Table VI. Thermogravimetric Vapor Pressure Results

Alloy	T (K) (Sol./Liq.)	Loss (mg)	P (atm) Pd, Au, or Ti	Activity Pd, Au, or Ti	$\Delta\overline{G}^{xs}/R$ (Kilokelvin)
V1. 70.7 ±3.9 at. pct Pd-Nb*	1974 (l)	401.0	7.1×10^{-5}	0.30	−1.7 ±1
V2. 71.3 ±3.3 at. pct Pd-Nb*	1954 (l)	339.0	8.1×10^{-5}	0.43	−1.0 ±1
V3. 71.6 ±3.0 at. pct Pd-Nb*	1877 (l)	212.0	2.8×10^{-5}	0.36	−1.3 ±1
V4. 75.1 ±0.1 at. pct Pd-Nb*	1693 (s)	6.4	2.3×10^{-7}	0.036	−5.1 ±1
V5a. 75.1 ±0.1 at. pct Pd-Zr*	1640 (s)	(0.6)	(1.6×10^{-8})	(0.006)	−8.0 ±4
V5b. 74.7 ±0.2 at. pct Pd-Nb*	1659 (s)	17.4	4.5×10^{-7}	0.12	−3.0 ±1
V6. 75.0 ±0.1 at. pct Pd-Zr*	1865 (s)	14.4	1.9×10^{-6}	0.028	−6.1 ±1
V7. 74.8 ±0.1 at. pct Pd-Zr*	1981 (s)	15.6	7.6×10^{-6}	0.030	−6.4 ±1
V8. 72.5 ±2.5 at. pct Au-Zr**	1668 (l)	525.0	7.7×10^{-6}	0.73	0 ±1
V9. 75.0 ±0.1 at. pct Au-Zr**	1487 (s)	8.0	9.2×10^{-8}	0.18	−2.1 ±1
V10. 74.8 ±0.2 at. pct Pd-Hf**	2010 (s)	20.2	4.8×10^{-6}	0.014	−8.0 ±1
V11a. 74.9 ±0.3 at. pct Pd-Zr**	1955 (s)	34.5	5.8×10^{-6}	0.030	−6.3 (±0.5 relative)
V11b. 74.7 ±0.3 at. pct Pd-Hf**	1955 (s)	31.9	5.2×10^{-6}	0.027	−6.5 (±0.5 relative)
V12. 56 ±19 at. pct Pd-Nb**	2050 (l)	662.0	1.7×10^{-4}	0.33	−1.1 ±1.8
V13. 66.1 ±8.8 at. pct Pd-Nb**	2058 (l)	568.0	1.6×10^{-4}	0.28	−1.8 ±1.7
V14a. 74.8 ±0.1 at. pct Pd-Hf**	2053 (s)	22.2	$(>9.1 \times 10^{-6})$	(>0.017)	(>−7.8 [±0.6 relative])
V14b. 75.0 ±0.2 at. pct Pd-Zr**	2053 (s)	24.2	$(>1.0 \times 10^{-5})$	(>0.019)	(>−7.5 [±0.6 relative])
V15a. 74.5 ±0.5 at. pct Pd-Ta**	1808 (s)	46.1	1.3×10^{-6}	0.038	−5.4 ±1 (±0.5 relative)
V15b. 74.5 ±0.4 at. pct Pd-Nb**	1761 (s)	670.0	1.7×10^{-6}	0.10	−3.5 ±1 (±0.5 relative)
V16a. 74.7 ±0.4 at. pct Pd-Ta**	1973 (s)	42.2	1.3×10^{-5}	0.055	−5.1 ±1 (±0.5 relative)
V16b. 74.8 ±0.1 at. pct Pd-Hf**	1973 (s)	6.2	1.9×10^{-6}	0.0081	−8.9 ±1 (±0.5 relative)
V17. 74.8 ±0.2 at. pct Ti-Ir***	2008 (l)	34.0	1.5×10^{-6}	0.11	−3.8 ±1.8

*Graphite Knudsen cell of purity 99.7 pct C.
**Graphite Knudsen cell of purity 99.99 pct C.
***16 gm 99.5 pct ThO_2 cell, 1.1 cm i.d. with no cell lid; no blank correction.

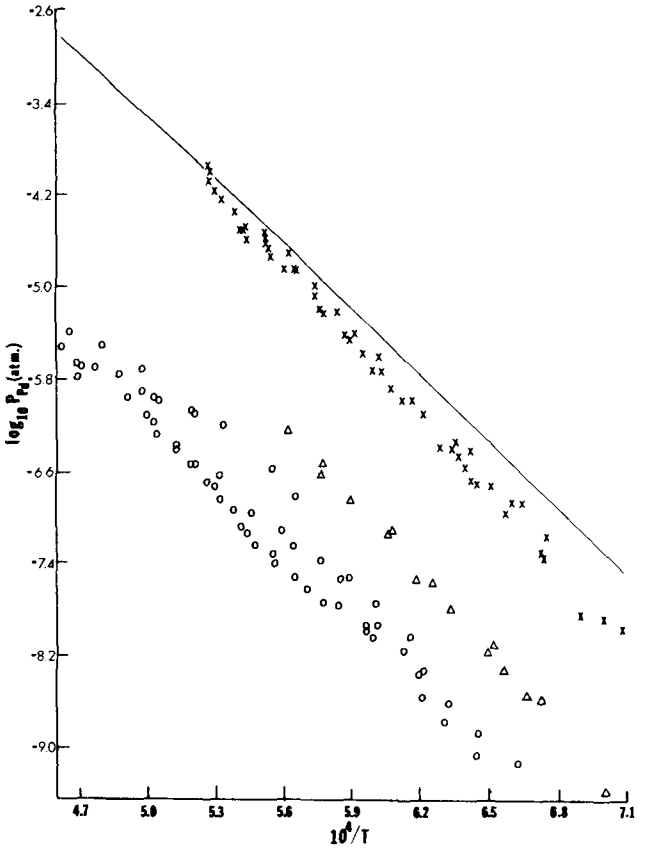

Fig. 5—Graphical representation of mass spectrometric vapor pressure results: — = pure Pd;[37] X = 82 at. pct Pd-Nb; Δ = 50 at. pct Pd-Nb; 0 = 20 at. pct Pd-Nb.

molal excess free energies for the volatile components; the absolute uncertainties include the uncertainties in the measured P (generally ±1.5×), and those in the values for P° (taken to be ±1.3×), while the relative uncertainties for comparison of two alloys run simultaneously include only a smaller version of the former (±1.3×). Alloys run simultaneously are so indicated by a letter following the same run number (*e.g.*, V11a and V11b). The log P_{Pd} *vs* $1/T$ plot of the data for the three Nb-Pd alloys studied mass spectrometrically includes the P°_{Pd} values selected by Hultgren, *et al.*;[37] the very high temperature results on the 20 at. pct Pd-Nb system are not included since severe Pd depletion was occurring.

Earlier equilibrations of ZrC with Pt and graphite[8] had been carried out at a somewhat lower temperature (1850 K) and starting only with pure Pt, so that the possibility of a diffusion-controlled product was raised. By starting with both a Zr-rich Zr-Pt alloy and pure Pt in separate runs and obtaining the same Zr Pt_3 product, it has been confirmed that this is the phase in equilibrium with ZrC and graphite. The emf data of Meschter and Worrell[7] give $\Delta\overline{G}_{Zr}/R$ (1300 K) = −45.5 kilokelvin for Pt-rich $ZrPt_3$, while extrapolation of the C-ZrC-$ZrPt_3$ equilibrium to that temperature yields $\Delta\overline{G}_{Zr}/R$ (1300 K) = −22.1 kilokelvin, so that a very rapid variation of Zr activity across the narrow $ZrPt_3$ phase is suggested by this result. Equilibration was similarly confirmed for the Nb-Pd system, and it is highly probable that equilibrium had been attained for all of the other runs. The temperature insensitivity of these equilibria is illustrated by comparing, for example, run C3 with C5 and C4 with C6; that the same MPl_3 intermetallic is in equilibrium with the carbide and graphite over a several

hundred degree range reflects a small $\Delta\bar{S}_M$ (and thus a small $\Delta\bar{H}_M$, since $\Delta\bar{G}_M = 0$ at equilibrium) for the transfer of the metal from its solid carbide to a solid or liquid alloy. Although entropy effects are clearly more significant for the very dilute alloys, the temperature sensitivity there is still expected to be small relative to the other uncertainties involved (particularly those in the carbide thermodynamic quantities). Since $\Delta\bar{S}^{xs}_{M(alloy)}$ should also be small, $\Delta\bar{G}^{xs}_M$ is close to $\Delta\bar{H}_M$ and will vary only slowly with temperature, so that comparisons of results obtained within a few hundred degrees of one another are reasonable. The production of MPl_3 intermetallics with rather similar $\Delta\bar{G}^{xs}_M$ in runs C1-10 does not allow for particularly useful comparisons between those systems, except perhaps that Ta may be a somewhat less effective acid with Ir than either Zr or Hf. Based upon the solid solution results, it is clear that Nb (C18-20) is a less effective acid with Pd than is Ta (C8) and W is only a weak acid with Ir (C12) and exhibits a repulsive interaction with Os (C16). Since the concentration of Zr in Os (C13) was below the EPMA detection limit, only a limit was established there, but this and the Zr-Ru result nonetheless serve to clarify the earlier work which suggested a greater stabilization of Zr in Ru than in its 5*d* analogue, Os. It is useful to compare the excess partial molal Gibbs energies extrapolated to zero concentration corresponding to the solute or Henry's Law standard states to remove the effect of composition as a variable. Brewer and Wengert[8] have described extrapolation procedures using the Gibbs-Duhem equation along with various solution models. When x_{Zr} is small and the extrapolation is short, it is adequate to assume a proportionality to the square of the mole fraction of the solvent and $\Delta\bar{G}^{xs,\infty} = (\Delta\bar{G}^{xs})/(1 - x)^2$. The two new data have been used to update the plot of $\Delta\bar{G}^{xs,\infty}_{Zr}$ (partial molal excess free energy of Zr at infinite dilution) *vs* atomic number of second and third series platinum group elements given by Brewer and Wengert,[8] and the combined results are shown in Figure 6. The dotted curves are included to suggest the possible shape of the actual stability curves, since only limits are available for several systems; the maximum in the second series stability hump is skewed slightly toward Pd,

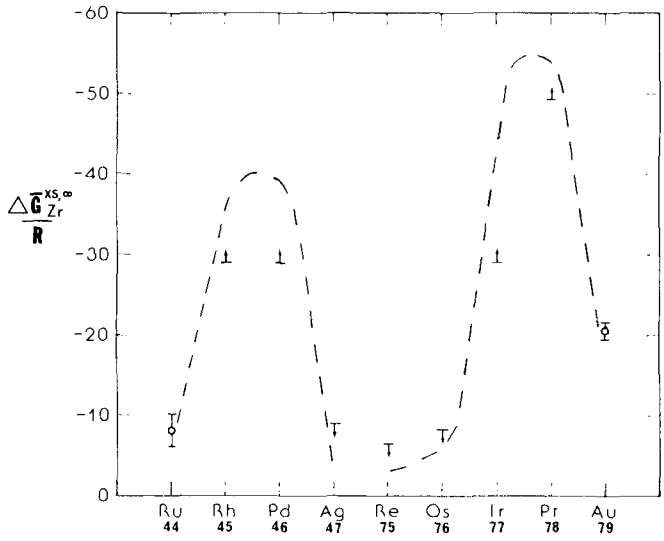

Fig. 6—Excess partial molal free energies in kilokelvin of zirconium at infinite dilution in second and third transition series platinum group elements at 1800 K.

based upon considerations discussed below regarding the relative effectiveness of Pd and Rh as donor elements. As discussed in the original paper,[8] this plot clearly suggests stability maxima between Rh and Pd for the second series and between Ir and Pt for the third. The data obtained here for Ta, Zr, Hf, and Nb with Os (runs C11, C13, C14, and C15) may imply a maximum in acceptor effectiveness at group IVB.

The nitride equilibria also exhibited only small temperature dependences (compare run N5 with N6, N9 with N13, and N15 with N17) and further showed a nitrogen pressure dependence generally smaller than the compositional uncertainties inherent in the analyses. Even a two-order magnitude variation in P_{N_2} at essentially constant temperature (one order variation in the a_M; compare run N5 with N8, and N10 with N11) resulted in Zr-Pt and Ti-Pt concentration changes smaller than the assigned uncertainties and in the wrong direction in the former case (increasing a_{Zr} resulting in decreasing X_{Zr}). The activity of the acid metal must be changing very rapidly with composition for these stable acid-base systems. Both Zr_3Pt_2 and pure Pt equilibrated with ZrN at ~2350 K under 1 atm N_2 resulted in the same equilibrium alloy, thus excluding the possibility of a diffusion-controlled product; equilibration was also confirmed for the NbN-NbPd system. Although it is difficult to make any quantitative comparisons between the Ti- , Zr- , and Hf-Pt systems given the rather poor resolution of these experiments, it does seem that the Ti-Pt interaction is at least somewhat weaker than the others. The Zr-Pt results are consistent with those from the carbide equilibrations, in that a slightly Zr-richer alloy (~30 at. pct Zr-Pt; run N7) has a slightly more positive $\Delta\bar{G}^{xs}_{Zr}/R$ ($\simeq -17.4$ kilokelvin) than does $ZrPt_3$ (run C9; $\Delta\bar{G}^{xs}_{Zr}/R \simeq -19.5$ kilokelvin). One clear comparison provided by these results is that Nb is a less effective acid with Pt (run N1) than are Ti, Zr, or Hf. Also, Pt is a more effective donor to Nb than is Pd (runs N18-20).

The large uncertainty assigned to thermogravimetric run V5a in Table VI reflects the total weight loss of only 1.6 mg corrected for blank loss to 0.6 mg with an uncertainty of ±1 mg. Due to an unexpected termination of power to the furnace, only limits were obtained from run V14, but these results are useful for comparing the 75 at. pct Pd-Hf and 75 at. pct Pd-Zr systems, since both alloys were maintained at temperature for the same (unknown) length of time. Although most of the temperature trends are in the expected direction of increasing a_M with increasing T and all are reasonable when the assigned uncertainties are considered, it is clear that no meaningful Second Law enthalpies may be obtained from these data. Since $\Delta\bar{S}^{xs}_M$ is expected to be small for these condensed alloys, $\Delta\bar{G}^{xs}_M$ should provide a rather good measure of $\Delta\bar{H}_M$. Consideration of alloys run simultaneously provides the following comparisons of acceptor metal effectiveness for M in MPd_3 alloys: Hf ≃ Zr (runs V11, V14); Ta > Nb (run V15); Hf > Ta (run V16); and, from the first and last comparisons, Zr > Ta. There seems to be a distinct maximum in acid effectiveness at group IVB and, although the *d* orbital extension effect is clearly apparent in comparing Nb (4*d*) with Ta (5*d*), it is not significant in comparison of Zr (4*d*) with Hf (5*d*); the bonding effectiveness of the sole vacant valence *d* orbital available to Nb/Ta may be particularly susceptible to the effects of contraction because of the crystal field effect discussed

above. The relative ineffectiveness of Au as a donor to Zr in $ZrAu_3$ compared with Pd in $ZrPd_3$ (runs V6 and V8) is taken as due to its higher nuclear charge. Kleykamp[48] performed emf measurements on Rh-rich $NbRh_3$ at 1200 K and found $\Delta\overline{G}^{xs}_{Rh}/R = -0.2$ kilokelvin, as compared with $\Delta\overline{G}^{xs}_{Pd}/R = -3.0 \pm 1$ kilokelvin in $NbPd_3$ at 1660 K established here. This comparison suggests that Pd is a more effective donor metal than is Rh, this presumably due to the availability of two non-bonding valence *d* electron pairs on the former, compared with only one pair on the latter.

The scatter in the log P_{Pd} *vs* $1/T$ data plotted in Figure 5 for each of the three Nb-Pd alloys studied mass spectrometrically is too large to obtain enthalpies from the best straight line fit, particularly since the quantity of interest ($\Delta\overline{H}_{Pd[alloy]}$) corresponds to the relatively small differences in slopes between the solid line (ΔH°_{vap} for pure Pd) and each of the three data sets ($\Delta\overline{H}_{vap,Pd[alloy]}$). Where the data for the 82 at. pct Pd-Nb alloy breaks through the P° curve, an activity of slightly greater than unity is implied; this unreasonable result is taken to reflect the uncertainty in the $P_{Pd[alloy]}$ data and/or the P°_{Pd} values used. The melting point of the 82 at. pct Pd-Nb system was repeatedly observed at 1822 ± 10 K ($10^4/T = 5.49$) with no significant break in P_{Pd}. The 50 at. pct Pd-Nb alloy did not melt up to the highest temperature attained of 1778 K. Data obtained on the 20 at. pct Pd-Nb system above 2128 K ($10^4/T = 4.7$) are not included in Figure 5, since the rapidly falling P_{Pd} at higher temperatures is simply taken to reflect the further depletion of Pd from that already Pd-poor alloy. A few Nb pressures were also obtained at these high temperatures, and the approximately unit Nb activity measured at approximately 2500 K is in accord with the final alloy composition of >99 pct Nb-Pd as established by EPMA of the post-run alloy.

The best straight line fit to the more reliable low temperature (1400 to 1800 K) data was made for each of the three data sets, and $\Delta\overline{G}^{xs}_{Pd}/R$ at 1515 K were obtained from these curves as: −1 kilokelvin for 82 at. pct Pd-Nb; −5.5 kilokelvin for 50 at. pct Pd-Nb; and −7.1 kilokelvin for 20 at. pct Pd-Nb. Again, these $\Delta\overline{G}^{xs}$ are expected to be dominated by $\Delta\overline{H}$ and thus provide a good measure of the thermal stabilization of Pd in the alloys relative to pure Pd. The large increase in stabilization which occurs upon dilution from 82 at. pct Pd-Nb to 50 at. pct Nb-Pd is taken to reflect the titration of the most effective of the two non-bonding pairs of Pd valence *d* electrons into the single available vacant valence *d* orbital of Nb. That only a relatively small additional stabilization (bonding) is seen upon further dilution suggests that the second pair of non-bonding valence *d* electrons of Pd is relatively ineffective in acid-base bonding, this presumably due to a crystal field effect, as discussed above. This interpretation is in accord with the $NbPd_3$ *vs* $NbRh_3$ comparison presented above, since the non-bonding valence *d* electrons available to Rh are in the least bonding-effective orbital for that series.

IV. CONCLUSION

These thermodynamic studies of several acid-base stabilized alloys may be interpreted in terms of the considerations outlined in the Introduction, and the following conclusions result:

1. Valence *d* electron donor and acceptor bonding effectiveness does increase upon moving down a given group, but this effect does not appear to be particularly pronounced in comparing certain second and third series elements, such as Zr and Hf.
2. The maximum in donor effectiveness probably occurs at Pd/Pt while the best acids are Zr and Hf; this may be interpreted in terms of a crystal field splitting which renders the last unused valence *d* orbital particularly ineffective in bonding, and is consistent with the partial titration curve (a_{Pd} *vs* X_{Pd}) obtained for the Nb-Pd system.

NOTATION

A	Area of Knudsen cell orifice
a_i	Thermodynamic activity of species i
dw/dt	Mass loss per unit time
E	Relative ionization efficiency
EPMA	Electron probe microanalysis
ΔG°_f	Standard free energy of formation
$\Delta\overline{G}_i$	Partial molal free energy change for transferring i from its standard state (pure i) to some mixture.
$\Delta\overline{G}^{xs}_i$	Excess partial molal free energy change ($= \Delta\overline{G}_i + T\Delta\overline{S}^{id}_i$)
ΔH°_f	Standard enthalpy of formation
I^+_i	Ion current for species i^+
k_i	Mass spectrometer pressure calibration constant for species i
M	Group IVB-VIB element
M_i	Molecular weight of species i
n	Isotopic abundance
P°_i	Vapor pressure of species i over the pure condensed standard state
Pl	Platinum group element
R	Ideal gas constant
$\Delta\overline{S}^{id}_i$	Ideal (configurational) partial molal entropy change
X_i	Mole fraction of species i
XRD	X-ray diffraction
$\pm AX$	Uncertainty range corresponding to the reported value $\div A$ to the reported value $\cdot A$
γ_i	Electron multiplier gain or activity coefficient for species i, as indicated in text
σ	Ionization cross section

ACKNOWLEDGMENT

This work was supported by the Division of Materials Sciences, Office of Basic Energy Sciences, United States Department of Energy under contract No. DE-AC03-76SF00098.

REFERENCES

1. N. Engel: *Ingenioeren*, 1939, Sect. M, p. 101 and 1940, Sect. M, p. 1; *Powder Met. Bull.*, 1954, vol. 7, pp. 8-18; *ASM Trans.*, 1964, vol. 57, pp. 610-19; *Acta Metall.*, 1967, vol. 15, pp. 557-63.
2. L. Brewer: in *High Strength Materials*, V. F. Zackay, ed., John Wiley and Sons, New York, NY, 1965, chap. 2, pp. 12-103.
3. L. Brewer: *Acta Metall.*, 1967, vol. 15, pp. 553-56; *Science*, 1968, vol. 161, pp. 115-22.
4. V. Srikrishnan and P. J. Ficalora: *Metall. Trans.*, 1974, vol. 5, pp. 1471-75.

5. L. Pauling: *The Nature of the Chemical Bond*, 3rd ed., Cornell Univ. Press, Ithaca, NY, 1960, pp. 93, 410.
6. L. Brewer: in *Phase Stability in Metals and Alloys*, P. Rudman, J. Stringer, and R. I. Jaffe, eds., McGraw-Hill Book Co., New York, NY, 1967, pp. 39-61.
7. P. J. Meschter and W. L. Worrell: *Metall. Trans. A*, 1976, vol. 7A, pp. 299-305; *Metall. Trans. A*, 1977, vol. 8A, pp. 503-09.
8. L. Brewer and P. R. Wengert: *Metall. Trans.*, 1973, vol. 4, pp. 83-104.
9. Ya. I. Gerassimov, V. I. Lavrentev, O. von Goldbeck, D. T. Livey, R. Ferro, and A. L. Dragoo: *Tantalum: Phusico-Chemical Properties of its Compounds and Alloys*, Special Issue No. 3, International Atomic Energy Agency, Vienna, 1972, pp. 44, 49.
10. H. L. Schick: *Thermodynamics of Certain Refractory Coupounds*, Academic Press, New York, NY, 1966, vol. 2, pp. 83-84.
11. E. Storms, B. Calkin, and A. Yencha: *High Temp. Science*, 1969, vol. 1, pp. 430-55.
12. W. L. Worrell and J. Chipman: *J. Phys. Chem.*, 1964, vol. 68, pp. 860-66.
13. E. K. Storms and J. Griffin: *High Temp. Science*, 1973, vol. 5, pp. 291-310.
14. P. J. Spencer, O. Kubaschewski-von Goldbeck, R. Ferro, R. Manazza, K. Girgis, and O. Kubaschewski: *Hafnium: Physico-Chemical Properties of its Compounds and Alloys*, Special Issue No. 8, International Atomic Energy Agency, Vienna, 1981, pp. 30-32.
15. *JANAF Thermochemical Data*, The Dow Chemical Co., Midland, MI: C ref. state, 1978; Hf ref. state, 1979; N_2 ref. state, 1977.
16. V. I. Lavrentev, Ya. I. Gerassimov, P. Feschotte, D. T. Livey, O. von Goldbeck, H. Nowotny, K. Siefert, R. Ferro, and A. L. Dragoo: *Niobium: Physico-Chemical Properties of its Compounds and Alloys*, Special Issue No. 2, International Atomic Energy Agency, Vienna, 1968, p. 26.
17. R. Hultgren, P. D. Desai, D. T. Hawkins, M. Gleiser, and K. K. Kelley: *Selected Values of the Thermodynamic Properties of Binary Alloys*, ASM, Metals Park, OH, 1973, pp. 1170-76.
18. C. B. Alcock, K. T. Jacob, S. Zador, O. Kubaschewski-von Goldbeck, H. Nowotny, K. Siefert, and O. Kubaschewski: *Zirconium: Physico-Chemical Properties of its Compounds and Alloys*, Special Issue No. 6, International Atomic Energy Agency, Vienna, 1976, p. 28.
19. M. Battuelo and T. Ricolfi: *High Temp.-High Pres.*, 1980, vol. 12, pp. 247-52.
20. Y. S. Touloukian and D. P. DeWitt: *Thermophysical Properties of Matter*, IFI/Plenum Data Corp., New York, NY, 1972, vol. 8, pp. 12, 1058, 1080, and 1086.
21. C. E. Holcomb: U.S.A.E.C. Oak Ridge Y-12 Plant, Report Y1887, 1973, reported in Ref. 32.
22. A. Amendola: Polytechnic Inst. of Brooklyn, NY, 1958, reported in Ref. 32.
23. T. F. Chase and E. F. Juenke: General Electric, Cincinnati, OH, 1968, reported in Ref. 32.
24. P. G. Cotter and J. A. Kohn: *J. Am. Cer. Soc.*, 1954, vol. 37, pp. 415-20.
25. J. M. Bind and G. J. McCarthy: Pennsylvania State University, 1973, reported in Ref. 32.
26. E. Raub and G. Falkenburg: *Metallwissenschaft und Technick*, 1973, vol. 27, pp. 669-79.
27. A. E. Dwight and P. A. Beck: *Trans. TMS-AIME*, 1959, vol. 215, pp. 967-79.
28. J. W. Downey: Met. Div., Argonne Nat'l. Lab., 1964, reported in Ref. 32.
29. J. B. Darby, J. W. Downey, and L. J. Norton: *TMS-AIME*, 1963, vol. 227, pp. 1028-29.
30. A. Raman and K. Schubert: *Z. Metalk.*, 1964, vol. 55, pp. 704-10.
31. J. W. Colby: *MAGIC IV—a computer program for quantitative electron microprobe analysis*, Bell Telephone Labs., Murray Hill, NJ, 1972.
32. *JCPDS Powder Diffraction Files*, International Centre for Diffraction Data, Swarthmore, PA, 1945 and after.
33. L. S. Birks: *Electron Probe Microanalysis*, 2nd ed., John Wiley and Sons, Inc., New York, NY, 1971, pp. 101-20.
34. J. I. Goldstein and J. W. Colby: in *Practical Scanning Electron Microscopy*, J. I. Goldstein and H. Yakowitz, eds., Plenum Press, New York, NY, 1975, pp. 435-89.
35. A. Taylor and N. J. Doyle: *J. Less-Common Metals*, 1967, vol. 13, pp. 413-30.
36. A. S. King: *Trans. Am. Electrochem. Soc.*, 1929, vol. 56, pp. 97-110.
37. R. H. Hultgren, P. D. Desai, D. T. Hawkins, M. Gleiser, K. K. Kelley, and D. D. Wagman: *Selected Values of Thermodynamic Properties of the Elements*, ASM, Metals Park, OH, 1973.
38. K. S. Pitzer and L. Brewer: revision of G. N. Lewis and M. Randall, *Thermodynamics*, 2nd ed., McGraw-Hill Book Co., New York, NY, 1961, p. 246.
39. R. C. Paule and J. L. Margrave: in *The Characterization of High Temperature Vapors*, J. L. Margrave, ed., John Wiley and Sons, Inc., New York, NY, 1967, pp. 130-51.
40. K. D. Carlson, P. W. Gilles, and R. J. Thorn: *J. Chem. Phys.*, 1963, vol. 38, pp. 2725-35.
41. J. P. Hirth: in *The Characterization of High Temperature Vapors*, J. L. Margrave, ed., John Wiley and Sons, Inc., New York, NY, 1967, pp. 453-72.
42. M. Knudsen: *Ann. Physik*, 1909, vol. 28, pp. 75-130.
43. G. L. Selman, P. J. Ellison, and A. S. Darling: *Platinum Metals Review*, 1970, vol. 14, pp. 14-20.
44. K. A. Gingerich: in *Current Topics in Materials Science*, E. Kaldis, ed., North Holland Publishing Company, New York, NY, 1980, vol. 6, pp. 345-462.
45. K. A. Gingerich: *J. Chem. Phys.*, 1968, vol. 49, pp. 14-18.
46. K. Hilpert and K. A. Gingerich: *Ber. Bunsenges Phys. Chem.*, 1980, vol. 84, pp. 739-45.
47. J. B. Mann: *J. Chem. Phys.*, 1967, vol. 46, pp. 1646-51.
48. H. Kleykamp: *J. Less-Common Metals*, 1982, vol. 83, pp. 105-13.